Bioorganic & Medicinal Chemistry xxx (xxxx) xxx–xxx

Contents lists available at ScienceDirect

Bioorganic & Medicinal Chemistry

journal homepage: www.elsevier.com/locate/bmc

Binding pocket-based design, synthesis and biological evaluation of novel selective BRD4-BD1 inhibitors

Junlong Ma[a,b], Heng Chen[a], Jie Yang[a], Zutao Yu[a], Pan Huang[a], Haofeng Yang[a], Bifeng Zheng[a], Rangru Liu[c], Qianbin Li[a], Gaoyun Hu[a], Zhuo Chen[a,*]

[a] Department of Medicinal Chemistry, Xiangya School of Pharmaceutical Sciences, Central South University, Changsha 410013, Hunan, PR China
[b] Department of Good Clinical Practice, Taihe Hospital, Hubei University of Medicine, Shiyan 442000, Hubei, China
[c] Key Laboratory of Tropical Diseases and Translational Medicine of the Ministry of Education & Hainan Provincial Key Laboratory of Tropical Medicine, Hainan Medical College, Haikou, China

ARTICLE INFO

Keywords:
BRD4
BD1 inhibitor
Cancer
Fibrosis
Computer-aided drug design
Structure-activity relationship

ABSTRACT

Bromodomain-containing protein 4 (BRD4), consisting of two tandem bromodomains (BD1 and BD2), is key epigenetic regulator in fibrosis and cancer, which has been reported that BD1 and BD2 have distinct roles in post-translational modification. But there are few selective inhibitors toward those two domains. Herein, this study designed and synthesized a series of novel selective BRD4-BD1 inhibitors, using computer-aided drug design (CADD) approach focused on exploring the difference of the binding pockets of BD1 and BD2, and finding the His437 a crucial way to achieve BRD4-BD1 selectivity. Our results revealed that the compound **3u** is a potent selective BRD4-BD1 inhibitor with IC_{50} values of 0.56 μM for BD1 but > 100 μM for BD2. The compound exhibited a broad spectrum of anti-proliferative activity against several human cancer and fibroblastic cell lines, which might be related to its capability of reducing the expression of c-Myc and collagen I. Furthermore, it could induce apoptosis in A375 cells. To the contrary, the selective BD2 inhibitor, RVX-208, did not indicate any of these activities. Our findings highlight that the function of BRD4-BD1 might be predominant in fibrosis and cancer. And it is rational to further develop novel selective BRD4-BD1 inhibitors.

1. Introduction

Bromodomain-containing protein 4 (BRD4), firstly identified in 1988 as a subset of epigenetic “reader”, is a member of the bromodomain and extra-terminal (BET) protein family.[1] In the past few years, compared with other BET family proteins (BRD2, BRD3 and BRDT), BRD4 has been most extensively studied because of its unique relevance with a number of human diseases including cancer, inflammation, cardiovascular diseases and multiple organ fibrosis.[2–4] Normally, BRD4 localizes in the nucleus and recruits positive transcriptional elongation factor complex (P-TEFb) to regulate RNA polymerase II activity, via binding to ε-*N*-acetylated lysine residues of histone.[5–7] In this way, BRD4 has the advantages of directly controlling downstream gene expression responsible for cellular proliferation and inflammatory pathways. For instance, BRD4 can directly promote transcription of the c-Myc oncogene and further increase the expression of c-Myc targeting genes, which play a crucial role in cancer pathogenesis.[8–11] In addition, BRD4 is also reported to play important roles in fibrosis via directly binding to the enhancer of collagen I, which is the main inducement of fibrosis.[4,12] Therefore, targeting BRD4 would be a potential strategy in cancer and fibrosis therapy.

Structurally, BRD4 contains a pair of bromodomains (BD1 and BD2), both of which are composed of a conserved fold consisting of four antiparallel helices (αZ, αA, αB, and αC) and two loop regions (ZA and BC loops) (Fig. 1).[13–15] The loop regions make up the pocket of the acetyl lysine (KAc) binding site, which is located at one end of the helix bundle. As for the difference of two tandem bromodomains, the amino acid sequence of BD1 and BD2 are conserved, achieving > 40% homology.[16] Especially at the site of binding pocket, there are only three crucial residues different from each other and show 95% sequence identity.[17] Although BD1 and BD2 show a high sequence similarity in the substrate-binding site, they specifically recognize different acetylation substrates in H3 and H4 histone tails.[18] And there have been some reports about the divergent function of BD1 and BD2. For example, the selective inhibition of BD1 can accelerate the differentiation of oligodendrocyte, which is opposite to the effect of non-selective inhibitor.[19] And it has been reported that BD2 could have broader effects toward other acetylated substrates, whereas BD1 tends to merely

* Corresponding author.
E-mail address: cz_job@csu.edu.cn (Z. Chen).

https://doi.org/10.1016/j.bmc.2019.03.037
Received 30 January 2019; Received in revised form 14 March 2019; Accepted 19 March 2019

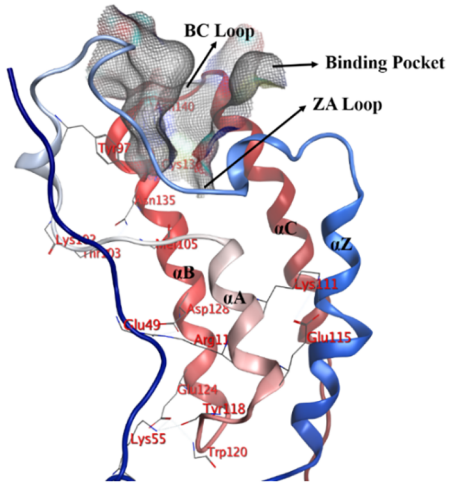

Fig. 1. The protein structure of BRD4-BD1 (PDB id: 2YEL).

recognizing H4 acetylation marks.[20,21] Consequently, in view of the different roles of BDs, it would be significant to design selective BRD4 inhibitors to explore whether BRD4-BD1 and BRD4-BD2 have different functions in diseases (such as cancer and fibrosis), which is beneficial to achieve more selective therapeutic effects.

Because of its comprehensive effects in disease, there have been several potent BRD4 inhibitors, some of which have been enrolled into different phases of human clinical trials (Fig. 2).[22–26] All of those inhibitors own a KAc mimic as hydrogen bond receptor, such as triazole, isoxazole and amide. Among them, RVX-208, as the first reported BD2 inhibitor, is now in phase III trial for the treatment of cardiovascular diseases owing to its upregulation of HDL-cholesterol and apolipoprotein A1 levels.[23] And Olionone, as one of few reported BD1 inhibitor, had potential off-target effect because of weak binding potency toward BRD4-BD1. However, except RVX-208 and Olionone, most of them are non-selective BRD4 inhibitors which can't discriminate the function of each bromodomain. Hence, it makes sense to design novel selective BRD4 inhibitor to explore the discrepant roles of BRD4-BD1 and BRD4-BD2. Here, we report the design, synthesis and biological evaluation of a new class of selective BRD4-BD1 inhibitors, thieno[2,3-*d*]pyrimidin-2(1H)-ones, which highlight the selective inhibition of BRD4-BD1 might be more efficient in the therapies of cancer and fibrosis.

2. Results and discussion

2.1. Design of target compounds

To design selective BRD4 inhibitor, the 3D crystal structure of the BRD4-BD1 and BRD4-BD2 at the binding pocket were superimposed (Fig. 3). The main structural difference is that the Asp144 in the BC loop of BRD4-BD1 is replaced by a histidine in BRD4-BD2 (His 437). Because the unique His437 in BRD4-BD2 flips into the KAc binding pocket, the BRD4-BD2 cavity is narrower than that of BRD4-BD1. This transformation of space can be exploited to design selective inhibitors. For example, RVX-208 exhibits tighter affinity towards BRD4-BD2 for its structural complementarity with narrow binding pocket.[23] To the contrary, few molecules such as Olionone prefers to bind to BRD4-BD1 because of structural clash with His437 in BRD4-BD2.[27]

Hence, it was hypothesized that an additional insert of steric hindrance moiety towards the His437 in BRD4-BD2 on the non-selective BRD4 inhibitors might generate BRD4-BD1 selectivity. Firstly, (+)-JQ1 was chosen as the lead compound core for its high potency[25]. As seen from cocrystal binding mode of (+)-JQ1 with BRD4 (Fig. 4a, b), a *tert*-butyl acetate part exposed to the cavity, which have no binding effect with receptor. The main interaction is that triazole in (+)-JQ1 extends into the inside of pocket and acts as H-bond acceptor with the Asn140 of BRD4-BD1 or the Asn433 of BRD4-BD2. Meanwhile the chlorobenzene part has hydrophobic interaction with WPF region (Trp81/374, Pro82/375 and Phe83/376). Hence, in our design, the H-bond acceptor part and phenyl group were reserved in the novel scaffold building. To avoid probable adverse effects in central nervous system of azapine scaffold, the azapine ring was directly replaced by pyrimidinone group. Consequently, the alkyl group, a steric hindrance moiety clashing with His437 of BRD4-BD2, was imported into the thiophene moiety, which expected to achieve BRD4-BD1 selectivity. The initial structure conception is shown in Fig. 4c.

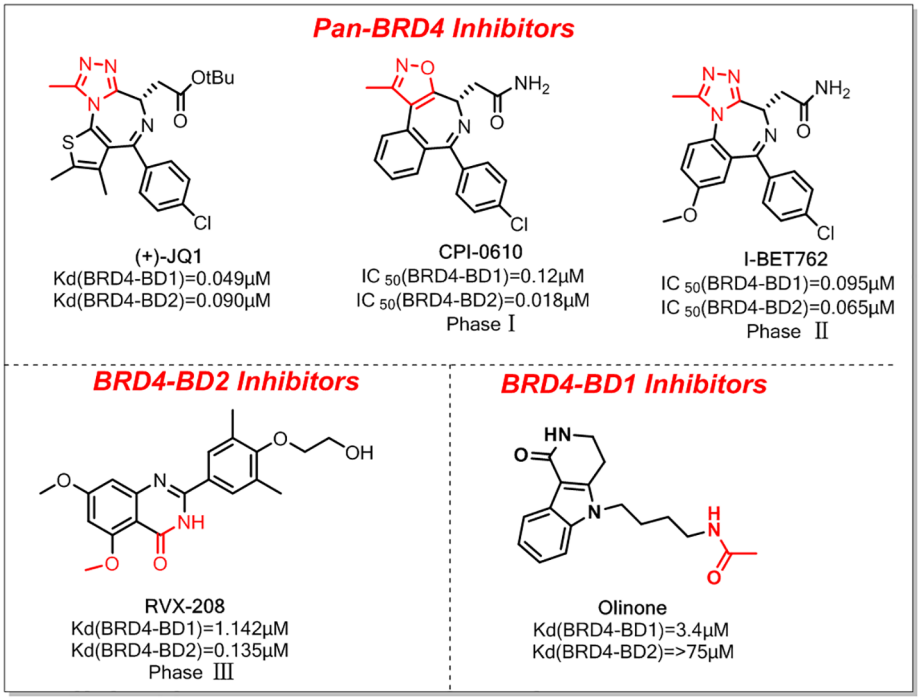

Fig. 2. Chemical structures of typical BRD4 inhibitors.

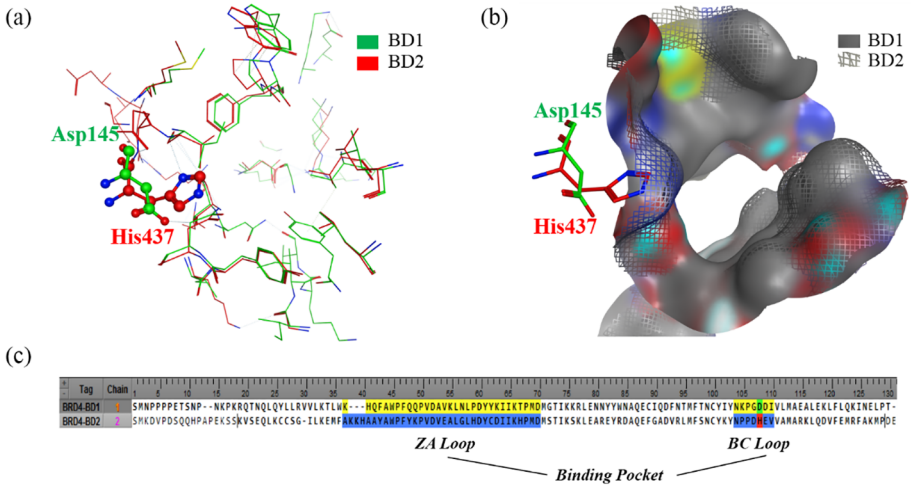

Fig. 3. Superimposition of BRD4-BD1 (PDB id: 2YEL) with BRD4-BD2 (PDB id: 2YEM) by residues (a, BD1 in green, and BD2 in red), binding pockets (b, BD1 in soild, and BD2 in line) and amino acid sequences(c). (For interpretation of the references to colour in this figure legend, the reader is referred to the web version of this article.)

2.2. Chemistry

Target compounds **3a–3z** were synthesized as outlined in Scheme 1. All compounds were purified by flash chromatography and purity was checked by high performance liquid chromatography (HPLC) before biological evaluation (purity was > 97%). The structures were confirmed by ^{1}H NMR, ^{13}C NMR spectrum and mass spectrometry.

As depicted in Scheme 1**,** an efficient route was developed to synthesize the compounds **3a–3z**. Firstly, via Gewald reaction, ketone reacted with benzoyl acetonitrile in ethanol to give the compounds **1a–1q**. The compounds **2a–2k** were obtained by cyclization of intermediate **1a–1q** with urea. By using the C—N coupling reaction between the intermediates **2a–2k** and substrates responsible for hydrogen bond receptors, the target compounds **3a–3z** were obtained. However, the defect of reaction C was the collateral products, O- substituted derivatives, which lead to the low yield. The order of reaction B and reaction C was reversed to get the single N- substituted compounds. Through the reaction D to reaction E, the target compounds were obtained with high yields.

2.3. BRD4 inhibitory assay and SAR study

AlphaScreen assay was used to evaluate BRD4 inhibitory activity of our compounds. (+)-JQ1 and RVX-208 were chosen as positive control. Initially, compound **3a–3h** were synthesized to preliminarily explore the influence of the spatial factors at thiophene part and the different hydrogen bond receptors at R_2 part. The results were shown in Table 1. With the increase in the bulk of part A from **3a** to **3d**, the inhibition rate and the selectivity between two *N*-terminal tandem bromodomains demonstrated that six-membered ring (**3c**) was the optimal substituent with 46.4% inhibition of BRD4-BD1 but 26.2% inhibition of BRD4-BD2 at 100 μM. If the ring was too small, it would have weak potency for BRD4. And if too big as seven members ring, it would lose the selectivity Then, the influence of different hydrogen bond receptors at **3c** and **3e–3h** were compared. It's obvious to find that heterocyclic isoxazole might be a preferable group to form hydrogen bond with asparaginate. Therefore, through the above initial structure-activity relationship (SAR) analysis, the compound **3c** was identified as the lead compound for further structural modification. Analyzing the docking conformation of **3c** with BRD4-BD1 and BRD4-BD2 (Fig 5a), we found

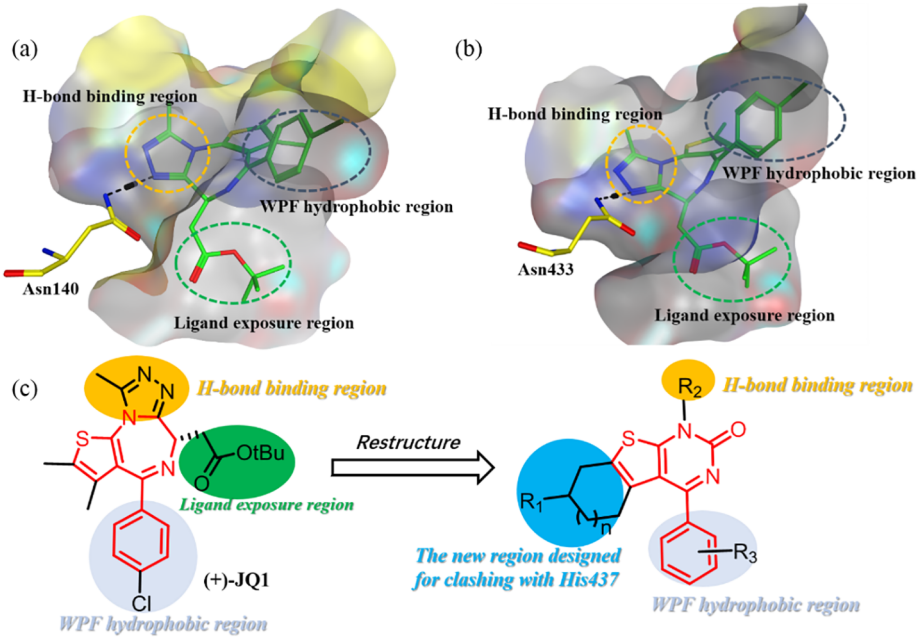

Fig. 4. (a) Docking conformation of (+)-JQ1 in BRD4-BD1 (PDB id: 2YEL). (b) Docking conformation of (+)-JQ1 in BRD4-BD2 (PDB id: 2YEM). (c) The conception of designing of the novel BRD4 inhibitors.

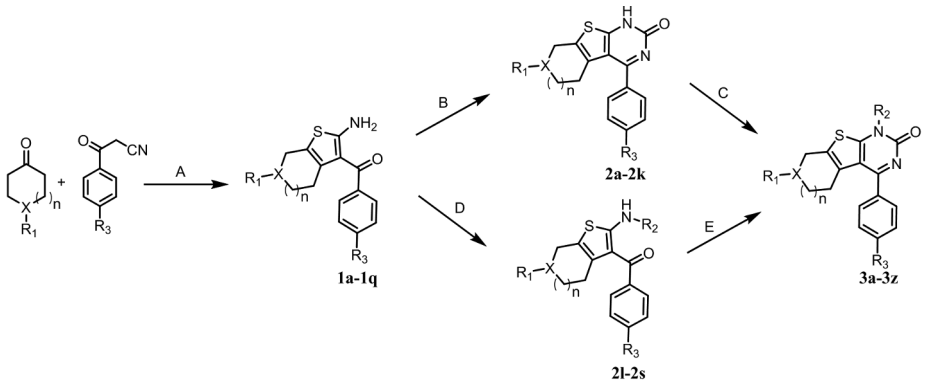

Scheme 1. General synthesis of **3a–3z**. Reagents and conditions: (A) S, EtOH, morpholine, 60 °C (B) NH_2CONH_2, 110 °C (C) K_2CO_3, DMSO, R_2Cl, 110 °C (D) K_2CO_3, CH_3CN, KI, R_2Cl 80 °C (E) NH_2CONH_2, MV 140 °C.

R_1 might be a crucial part to achieve selectivity because of its close distance with His437. Hence, R_1 was replaced by methyl formate, dimethyl, isopropyl, phenyl and *tert*-butyl. As shown in Table 1, **3o** with a *tert*-butyl group owned satisfactory potency and selectivity, with the IC_{50} value of 2.4 μM for BD1 and > 100 μM for BD2. To verify whether the selectivity is achieved by the reason of the clash with His437, the optimal conformation of **3o** was docked into the superposed BRD4-BD1 with BRD4-BD2 pocket (Fig 5b). It was obvious to find out that *tert*-butyl group was too closed with His437(BRD4-BD2) to be compatible with the pocket. Consequently, *tert*-butyl group was indispensable for the selectivity in structure.

In order to further improve the potency towards BRD4-BD1, we paid our attention to the WPF region of BRD4. It has been generally acknowledged that WPF region is crucial for the binding potency of inhibitors. As shown in Fig. 5a, b, a phenyl group was exactly located in this region. Hence, some hydrophobic groups (methoxy, methyl formate and halogen) were introduced. By comparing with the activity of **3o–3r** (Table 2), the electron donating group (**3p**) was weaken than the

Table 1
Chemical structure and BRD4 (BD1 and BD2) inhibitory activity of compounds **3a–3o**.

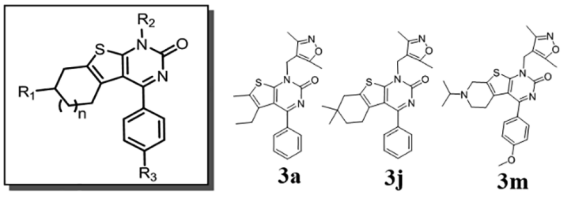

Comp.	Structure				IC50 (μM)[a] or (inhibitory rate[b])	
	n	R_1	R_2	R_3	BRD4-BD1	BRD4-BD2
3a					(9.5%)	(17.8%)
3b	0	-H		-H	(23.0%)	(19.8%)
3c	1	-H		-H	(46.4%)	(26.2%)
3d	2	-H		-H	(84.4%)	(81.2%)
3e	1	-H		-H	(23.7%)	(17.2%)
3f	1	-H		-H	(30.0%)	(13.6%)
3g	1	-H		-H	(38.5%)	(3.1%)
3h	1	-H	-Me	-H	(42.6%)	(66.2%)
3i	1	-COOMe		-H	(19.0%)	(9.0%)
3j					(86.6%)	(44.9%)
3k	1	-Ph		-Cl	6.0 ± 0.7	(15.1%)
3l	1	-Ph		-Cl	(44.9%)	(14.5%)
3m					(82.9%)	(66.6%)
3n	1	-tBu		-H	8.2 ± 0.4	(41.2%)
3o	1	-tBu		-Cl	2.4 ± 0.2	(23.4%)
(+)-JQ1[c]					0.17 ± 0.02	0.08 ± 0.01
RVX-208[c]				3.1 ± 0.12	0.10 ± 0.01	

[a] Data presented is mean ± SD value of three independent experiments.
[b] Inhibition rate mean values at a concentration of 100 μM were obtained from three independent experiments.
[c] Used as positive control.

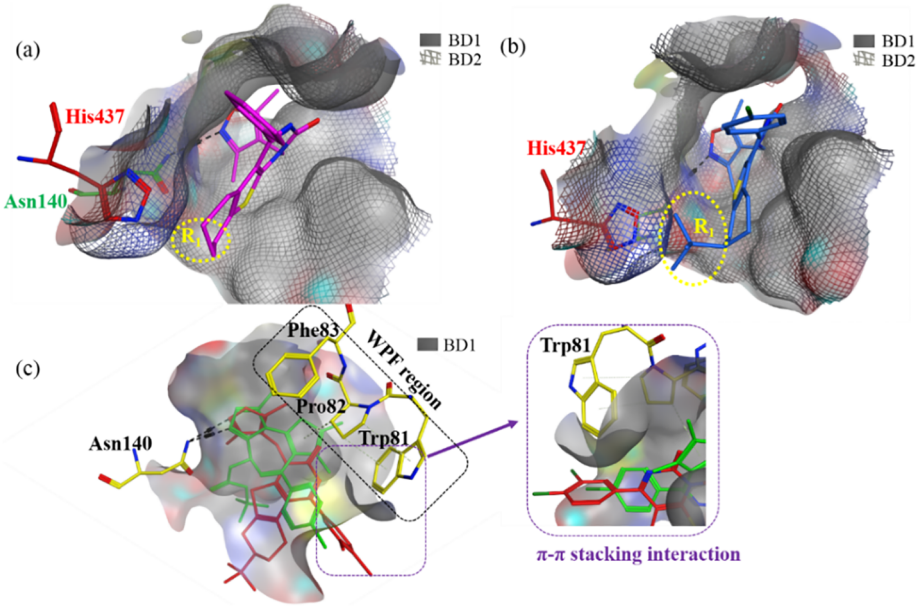

Fig. 5. (a) Docking conformation of **3c** in superimposition of BRD4-BD1 (PDB id: 2YEL) and BRD4-BD2 (PDB id: 2YEM). (b) Docking conformation of **3o** in in superimposition of BRD4-BD1 (PDB id: 2YEL) and BRD4-BD2 (PDB id: 2YEM). (c) Overlap of docking conformation of (+)-JQ1(green) and **3u** (red) in BRD4-BD1 (PDB id: 2YEL). (For interpretation of the references to colour in this figure legend, the reader is referred to the web version of this article.)

Table 2
Chemical structure and BRD4 (BD1 and BD2) inhibitory activity of compounds **3o–3z**.

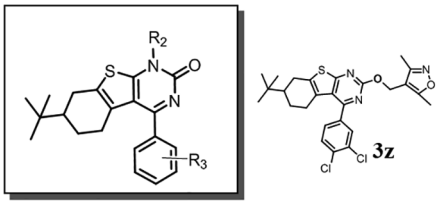

Comp.	Structure		IC_{50} (μM)[a] or (inhibitory rate[b])	
	R_2	R_3	BRD4-BD1	BRD4-BD2
3o		p-Cl	2.4 ± 0.2	(23.4%)
3p		p-OMe	11.4 ± 0.8	(42.2%)
3q		p-COOMe	1.5 ± 0.2	(49.7%)
3r		p-F	3.6 ± 0.5	(33.2%)
3s		m-Cl	3.1 ± 0.2	(52.3%)
3t		o-Cl	1.6 ± 0.2	(39.5%)
3u		p-Cl, m-Cl	0.56 ± 0.04	(29.9%)
3v		-H	(70.4%)	(66.6%)
3w		-H	22.7 ± 1.2	(28.3%)
3x		p-OMe	18.5 ± 1.4	(57.2%)
3y		p-Cl	n.d.[d]	n.d.[d]
3z			(32.6%)	(9.3%)
(+)-JQ1[c]			0.17 ± 0.02	0.08 ± 0.01
RVX-208[c]			3.1 ± 0.12	0.10 ± 0.01

[a] Data presented is mean ± SD value of three independent experiments.
[b] Inhibition rate mean values at a concentration of 100 μM were obtained from three independent experiments.
[c] Used as positive control.
[d] n.d. = not determined.

electron withdrawing groups (**3o, 3q and 3r**) and 4-chlorophenyl moiety (**3o**) was identified as the best substituent, which is the same group as (+)-JQ1's. For further modification, the substituents of chlorine were altered to the ortho and meta position of the phenyl group. Eventually, the compound **3u**, containing a 3,4-dichlorophenyl group, came out as the most suitable compound. Analyzing the docking conformation of (+)-JQ1 and **3u** with BRD4-BD1 (Fig. 5c), the 3,5-dimethylisoxazole of **3u** overlapped with the 3-methyl-1,2,4-triazole of (+)-JQ1, both of which acted as a KAc mimic. The introduction of 3,4-dichloro substituent made the plane of the 3,4-dichlorophenyl tend to be perpendicular to the plane of the pyrimidinone, which could have a π-π stacking interaction with the Trp81. To verify 3,5-dimethylisoxazole moiety is an effective KAc mimic, several different heterocycles were also designed as hydrogen bond receptors (**3v–3y)** (Table 2). Meanwhile, the compound **3z**, as the **O**-substituted isomer of the **3u**, was synthesized. By comparing the activities of these compounds, **3u** was reconfirmed as the most suitable compound for further biological activity evaluation.

In general, *tert*-butyl group was optimal at alkyl part (R_1) for BRD4-BD1 selectivity and 3,5-dimethylisoxazole moiety was the most effective KAc mimic which interacted with the crucial Asn140. As for WPF region, 3,4-dichloride might be the most suitable at phenyl substituent group (R_3) for improving potency.

2.4. Anti-cancer evaluation in vitro

It has been widely recognized that BRD4 is a desired target for the treatment of cancer. Accordingly, the anti-cancer activity of our compounds was firstly evaluated. Lung cancer cell line (A549), colon cancer cell line (HT-29), hepatoma cell line (HepG2) and melanoma cell line (A375) were employed to investigate the cancer cell growth-inhibitory activity. As shown in Table 3, a large portion of compounds could effectively inhibit the proliferation of these cancer cell lines at IC_{50} values ranging from 2.4 to 19.4 μM, which is similar to (+)-JQ1, the classic pan-BRD4 inhibitor. While, RVX-208, as the representative of selective BD2 inhibitor, showed low inhibition potency on these cancer cell lines, which initially implied different functions of BRD4-BD1 and BRD4-BD2 in cancer. And breast cancer cell line (MCF-7), which has been reported to be BRD4 inhibitor-resistant cell line,[28–30] was also employed to evaluate synthetic compounds. Compared the cell growth-inhibitory activity towards other cell lines, most of the synthetic compounds as

Table 3
Growth-inhibitory activities towards various cancer cell lines.

Comp.	Antiproliferative activity (IC_{50}, μM)[a]				
	A549	HT-29	HepG2	A375	MCF-7
3n	29.6 ± 1.8	20.1 ± 2.6	10.9 ± 2.0	8.0 ± 0.4	> 100
3o	66.5 ± 3.9	33.8 ± 2.7	26.4 ± 3.6	13.6 ± 1.2	78.3 ± 2.0
3p	18.9 ± 0.1	13.0 ± 1.0	15.1 ± 2.8	14.2 ± 1.8	10.4 ± 0.4
3q	19.3 ± 1.4	17.8 ± 3.2	12.8 ± 2.5	8.7 ± 1.5	38.6 ± 1.7
3r	49.9 ± 5.1	10.7 ± 1.3	63.7 ± 7.6	14.2 ± 1.0	33.3 ± 1.3
3s	18.9 ± 2.4	19.7 ± 2.0	3.6 ± 1.7	15.9 ± 0.8	25.7 ± 0.4
3t	16.6 ± 0.3	19.2 ± 1.6	30.0 ± 1.2	11.1 ± 1.5	69.2 ± 3.0
3u	24.5 ± 0.6	19.4 ± 0.1	14.5 ± 3.3	4.9 ± 1.4	16.6 ± 0.4
3w	31.9 ± 2.1	54.4 ± 6.3	2.4 ± 1.1	14.7 ± 2.7	> 100
3x	95.1 ± 7.6	98.0 ± 1.6	14.5 ± 1.3	6.5 ± 0.7	> 100
RVX-208[b]	53.1 ± 2.8	235.8 ± 36.4	103.0 ± 1.4	240.9 ± 51.2	> 300
(+)-JQ1[b]	13.1 ± 1.0	19.6 ± 1.9	11.3 ± 0.2	7.5 ± 0.3	38.0 ± 1.1

[a] Data presented is mean ± SD value of three independent experiments.
[b] Used as positive control.

well as (+)-JQ1 are both insensitive to MCF-7 cells, which indicated that the compounds inhibited the growth of cancer cells via binding to BRD4.

To further verify discrepant functions in cancer, compound **3u**, as the most potent selective BD1 inhibitor we've got, was proceeded to test the efficacy in A375 cells by measuring reduction of c-Myc, a well-known proto-oncogene in cancer progression which directly regulated by BRD4. A375 cells were treated with **3u**, (+)-JQ1 and RVX-208 at the concentration of 10 μM. As shown in Fig. 6a, 3u reduced the expression of the c-Myc in A375 cells at protein level in a dose-dependent manner. Significantly, it could be concluded that the selective inhibition of BD1 was sufficient to regulate the expression of c-Myc in A375 cells. These results were in consistent with the decrease of c-Myc at mRNA level (Fig. 6b). Both **3u** and (+)-JQ1 could inhibit the transcription of target gene at 10 μM, while RVX-208 was as the same as vehicle control group. In brief, these results suggested that the effect of BRD4-BD1 and BRD4-BD2 might be discrepant in cancer cells, and the inhibition of BRD4-BD1 rather than BRD4-BD2 could play a vital role in the regulation of oncogene.

Furthermore, the apoptosis-inducing activity related to c-Myc suppression on A375 cells was investigated, by which conducted double-staining with Annexin V-FITC and PI- and detected by the fluorescence microscope. As shown in Fig. 7, **3u** and (+)-JQ1 displayed similar ability to induce early apoptosis (the cytomembrane could be stained by Annexin V-FITC while cell nucleus could not be stained by PI in this state) of the cells both at the concentration of 10 μM. RVX-208 had no effect on apoptosis at the same concentration, which was in line with the weak inhibitory activity of c-Myc and the cell-viability data. In general, these results indicate the discrepant functions of BRD4-BD1 and BRD4-BD2 in the occurrence of cancer. And specific targeting single bromodomain of BRD4-BD1 is sufficient in the therapy of cancer.

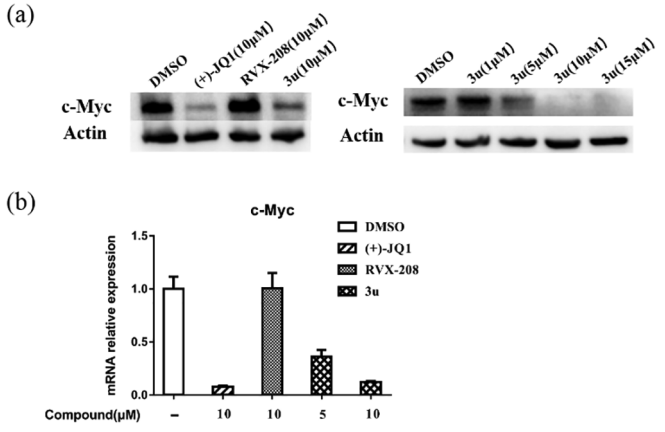

Fig. 6. Western blot and quantitative RT-PCR analysis of c-Myc.

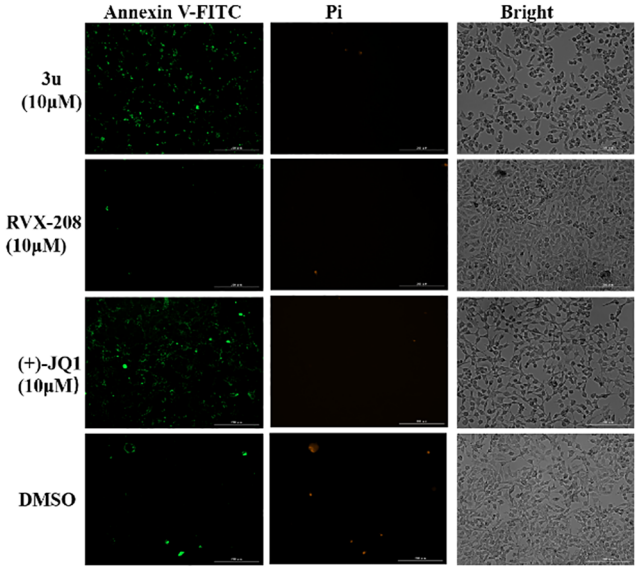

Fig. 7. Detection of apoptotic cells by Annexin V-FITC and PI double staining.

2.5. Anti-fibrotic evaluation in vitro

The vital role of BRD4 in fibrosis has been revealed in recent years. However, the detail functions of BRD4-BD1 and BRD4-BD2 on fibrotic development have not be specified yet. Here, it was explored whether the selective BRD4-BD1 inhibitors also have the abilities of anti-fibrosis as well as anti-cancer effects. Pulmonary fibroblastic cell line (HLF-1), renal fibroblastic cell line (NRK-49F) and liver fibroblastic cell line (LX-2) were chosen to investigate the fibrotic cell growth-inhibitory activity using MTT assay (Tables S1 and S2). As shown in Table 4, most of the compounds displayed potent anti-proliferative activities with average IC_{50} value ranging from 4.2 to 19.6 μM, which were more effective than (+)-JQ1 and RVX-208. And these data imply that BRD4 -BD1 may also be the primary factor in fibrosis.

In order to investigate the precise mechanism of anti-fibrosis, the inhibitory effect of **3u** to collagen I in HLF-1 cell line was assessed, which is the main component of the extracellular matrix (ECM) and a key factor in governing the course of fibrosis. The results displayed that **3u** dose-dependently inhibited the expression of collagen I and was more potent than (+)-JQ1 at the same concentration of 10 μM. To the

Table 4
Growth-inhibitory activities towards various fibroblastic cell lines.

Comp.	Antiproliferative activity (IC_{50}, μM)[a]		
	HLF-1	NRF-49F	LX-2
3n	21.3 ± 2.6	23.1 ± 3.6	21.6 ± 3.4
3o	18.9 ± 0.9	26.3 ± 0.8	10.4 ± 0.8
3p	14.1 ± 2.0	22.2 ± 0.8	12.9 ± 1.3
3q	6.6 ± 0.9	8.1 ± 0.9	19.6 ± 1.6
3r	14.5 ± 0.4	23.3 ± 0.8	17.3 ± 1.3
3s	12.8 ± 2.0	8.5 ± 2.0	15.3 ± 1.9
3t	12.0 ± 0.9	17.2 ± 2.3	11.3 ± 4.2
3u	13.6 ± 0.9	16.0 ± 1.1	9.1 ± 0.3
3w	7.6 ± 0.6	6.0 ± 1.6	4.2 ± 0.2
3x	14.6 ± 1.5	11.2 ± 2.4	12.4 ± 3.8
RVX-208[b]	52.0 ± 1.5	42.0 ± 2.9	79.7 ± 3.4
(+)-JQ1[b]	20.4 ± 1.8	21.1 ± 0.4	28.6 ± 4.1

[a] Data presented is mean ± SD value of three independent experiments.
[b] Used as positive control.

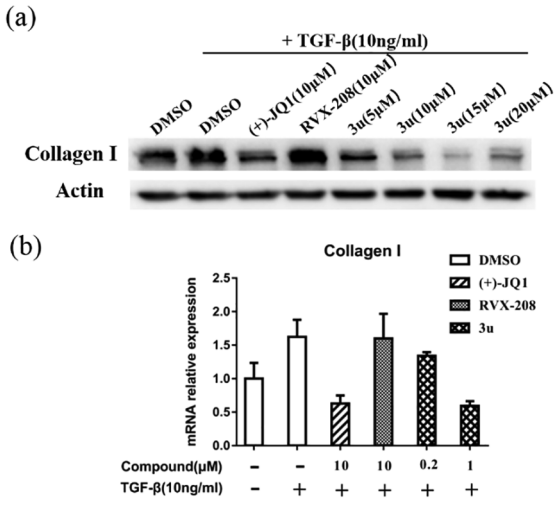

Fig. 8. Western blot and quantitative RT-PCR analysis of collagen I.

contrary, RVX-208 had no inhibition effect on the expression of collagen I (Fig. 8a). And quantitative RT-PCR assay was subsequently performed to verify the mRNA results. As expected, **3u** at 1 μM was as the potent as (+)-JQ1 at 10 μM in the inhibition transcription of collagen I, while this effect was not observed with RVX-208 treatment (Fig. 8b). Collectively, the mRNA level were in keeping with protein level, which may account for its anti-proliferative activity. In summary, all the experiments highlight that BRD4-BD1 plays the dominate role in the process of fibrosis and selectively inhibiting BRD4-BD1 can demonstrate more potent anti-fibrotic activity than the inhibition of both BRD4-BD1 and BRD4-BD2.

3. Conclusions

BRD4 plays a critical role in the development of cancer and fibrosis. And the close relevance of cancer and fibrosis, which is like the relationship between the seed and the soil, highlights the advantages of BRD4 and makes it a promising drug target. However, the specific functions of BRD4-BD1 and BRD4-BD2 are unclear in the occurrence of cancer and fibrosis. Until now, most of BRD4 inhibitors are non-selective. Especially for BD1, there are no potent selective inhibitors. Thus, there remains an urgent need to develop potent and selective BRD4-BD1 inhibitors for biological studies and disease therapeutics.

Herein, through preliminarily combining molecular docking and molecular dynamic study, a series of novel BRD4 inhibitors were designed and synthesized with high selectivity for BRD4-BD1 over BRD4-BD2 by the introduction of *tert*-butyl group, which would clash with the unique His437 of BRD4-BD2. SAR study led to the identification of **3u** as the most potent BRD4-BD1 inhibitory activities, which possessed high selectivity with IC_{50} values of 0.56 μM for BRD4-BD1 but > 100 μM for BRD4-BD2 Moreover, it showed a significant growth-inhibitory effect on multiple cancer cell lines as well as fibroblastic cell lines. The mechanism studies of anti-cancer and anti-fibrotic effects proved that **3u** could inhibit the transcription and translation of c-Myc and collagen I, while a selective BD2 inhibitor, RVX-208, had no significant inhibition. Hence, these results suggest that the BRD4-BD1 might be predominant in fibrosis and cancer, which encourage us to discovery the more potent selective BRD4-BD1 inhibitors to avoid any unwanted BRD4-BD2 dependent cellular effects that are unrelated to the treatments of cancer and fibrosis. Finally, **3u** could be used as a novel lead compound to further develop potent selective BRD4 inhibitors against organ fibrosis or cancer.

4. Experimental section

4.1. Chemistry section

4.1.1. A general method for synthesis of compounds *1a–1q*

3-oxo-3-phenylpropanenitrile (2.96 g, 20.4 mmol) and pentan-3-one (2.14 mL, 20.4 mmol) were put into 100 mL round bottom flask, then 50 mL ethyl alcohol chloride as solvent and 1 mL morpholine used as catalyst for the reaction were added. The reaction mixture was stirred at room temperature for 15 mins. Then sulphur (0.85 g, 26.6 mmol) was added to above mixture. The reaction mixture was heated at 60 °C for 12 h. The organic solvent was evaporated and the residue dissolved in ethyl acetate and purified with silica gel column chromatography (product eluted at 10% [v/v] ethyl acetate/petroleum ether) to afford (2-amino-4-ethyl-5-methylthiophen-3-yl)(phenyl) methanone(**1a**) as a yellow crystal.

4.1.2. A General method for synthesis of compounds *2a–2k*

(2-amino-4-ethyl-5-methylthiophen-3-yl)(phenyl)methanone(**1a**, 2 g, 8.2 mmol) and urea (0.98 g, 16.3 mmol) were put into 100 mL round bottom flask, then 40 mL acetic acid as solvent was added. The reaction mixture was heated at 110 °C for 12 h. The reaction mixture was then diluted with 150 mL ethyl acetate and washed with brine (75 mL × 3). The organic solvent was removed under vacuum. The mixture was dried to get the crude product of 5-ethyl-6-methyl-4-phenylthieno[2,3-d] pyrimidin-2(1H)-one (2a). The crude product was recrystallized with EtOH, filtered, and dried in vacuum to give pure product of 5-ethyl-6-methyl-4-phenylthieno[2,3-d] pyrimidin-2(1H)-one (**2a**) as a yellow crystal.

4.1.3. A general method for synthesis of compounds *2l* to *2s*

(2-amino-6-(*tert*-butyl)-4,5,6,7-tetrahydrobenzo[*b*]thiophen-3-yl) (3,4-dichlorophenyl) methanone(**1p**, 2 g, 5.2 mmol) and 4-(chloromethyl)-3,5-dimethylisoxazole (0.78 mL, 6.2 mmol) were put into 100 mL round bottom flask. Then 50 mL acetonitrile as solvent, 0.1 g potassium carbonate and 0.1 g potassium iodide used as catalyst for the reaction were added. The reaction mixture was heated at 80 °C for 4 h. The organic solvent was removed under vacuum. The mixture was dried to get the crude product of 5-ethyl-6-methyl-4-phenylthieno[2,3-d] pyrimidin-2(1H)-one (**2a**). The crude product was recrystallised with EtOH, filtered, and dried in vacuum to give pure product of (6-(*tert*-butyl)-2-(((3,5-dimethylisoxazol-4-yl)methyl)amino)-4,5,6,7-tetrahydrobenzo [b]thiophen-3-yl)(3,4-dichlorophenyl)methanone (**2s**) as a yellow crystal.

4.1.4. A General method for synthesis of compounds *3a–3z*

5-ethyl-6-methyl-4-phenylthieno[2,3-d] pyrimidin-2(1H)-one (**2a**, 2 g, 7.4 mmol) and 4-(chloromethyl)-3,5-dimethylisoxazole (0.94 mL, 8.9 mmol) were put into 100 mL round bottom flask, then 50 mL

dimethylsulfoxide as solvent and 0.1 g potassium carbonate used as catalyst for the reaction were added. The reaction mixture was heated at 110 °C for 1.5 h. The reaction mixture was then diluted with 100 mL dichloromethane and washed with brine (50 mL × 3). The organic solvent was removed under vacuum. The residue dissolved in ethyl acetate and purified with silica gel column chromatography (product eluted at 100% [v/v] ethyl acetate/petroleum ether) to afford 1-((3,5-dimethylisoxazol-4-yl)methyl)-5-ethyl-6-methyl-4-phenylthieno[2,3-*d*] pyrimidin-2(1H)-one (**3a**) as a yellow crystal.

*4.1.5. A General method for synthesis of compounds **3p–3q** and **3s–3u***

(6-(*tert*-butyl)-2-(((3,5-dimethylisoxazol-4-yl)methyl)amino)-4,5,6,7-tetrahydrobenzo[b] thiophen-3-yl)(3,4-dichlorophenyl)methanone (**2s**, 0.5 g, 1.0 mmol) and urea (0.12 g, 2.1 mmol) were put into 25 mL pressure flask, then 15 mL acetic acid as solvent was added. The reaction mixture was heated at 145 °C under microwave for 25 mins. The reaction mixture was then diluted with 30 mL ethyl acetate and washed with brine (20 mL × 3). The organic solvent was removed under vacuum. The mixture was dried to get the crude product 7-(*tert*-butyl)-4-(3,4-dichlorophenyl)-1-((3,5-dimethylisoxazol-4-yl)methyl)-5,6,7,8-tetrahydrobenzo[4,5]thieno[2,3-d]pyrimidin-2(1H)-one (**3u**). The crude product was recrystallized with EtOH, filtered, and dried in vacuum to give pure product of 7-(*tert*-butyl)-4-(3,4-dichlorophenyl)-1-((3,5-dimethylisoxazol-4-yl)methyl)-5,6,7,8-tetrahydrobenzo[4,5] thieno[2,3-d]pyrimidin-2(1H)-one (**3u**) as a yellow crystal.

*4.1.5.1. 1-((3,5-dimethylisoxazol-4-yl)methyl)-5-ethyl-6-methyl-4-phenylthieno[2,3-d]pyrimidin-2(1H)-one **(3a)***. Yellow solid, yield 82%, m.p. 163.6–165.8 °C; ^{1}H NMR (500 MHz, DMSO) δ 7.57–7.48 (m, 5H), 5.20 (d, J = 13.2 Hz, 2H), 2.45 (s, 3H), 2.31 (s, 3H), 2.12 (s, 3H), 2.09 (d, J = 7.2 Hz, 2H), 0.75–0.44 (m, 3H); ^{13}C NMR (126 MHz, DMSO) δ 168.99, 168.53, 159.44, 157.28, 154.37, 138.58, 133.99, 129.99, 128.38, 128.13, 126.26, 118.44, 108.17, 41.09, 20.02, 14.43, 12.83, 11.64, 10.58; HR-ESI-MS *m/z*: calcd for $C_{21}H_{22}N_3O_2S\{[M+H]^+\}$ 380.1433, found 380.1442.

*4.1.5.2. 1-((3,5-dimethylisoxazol-4-yl)methyl)-4-phenyl-1,5,6,7-tetrahydro-2H-cyclopenta[4,5]thieno[2,3-d] pyrimidin-2-one **(3b)***. Yellow solid, yield 75%, m.p. 166.7–168.8 °C; ^{1}H NMR (500 MHz, DMSO) δ 7.56 (ddd, J = 21.7, 15.1, 7.3 Hz, 5H), 5.20 (s, 2H), 2.84 (t, J = 6.4 Hz, 2H), 2.45 (s, 3H), 2.34 (d, J = 6.3 Hz, 2H), 2.22 (dd, J = 13.7, 6.9 Hz, 2H), 2.11 (s, 3H); 13C NMR (126 MHz, DMSO) δ 168.55, 168.00, 162.43, 159.42, 154.99, 138.87, 137.65, 134.17, 130.74, 129.02, 128.50, 114.96, 108.15, 40.99, 30.78, 29.21, 27.77, 11.63, 10.57; HR-ESI-MS *m/z*: calcd for $C_{21}H_{20}N_3O_2S\{[M+H]^+\}$378.1276, found 378.1283.

*4.1.5.3. 1-((3,5-dimethylisoxazol-4-yl)methyl)-4-phenyl-5,6,7,8-tetrahydrobenzo[4,5]thieno[2,3-d]pyrimidin-2(1H)-one **(3c)***. Yellow solid, yield 82%, m.p. 184.1–186.6 °C; ^{1}H NMR (500 MHz, DMSO) δ 7.57–7.46 (m, 5H), 5.19 (s, 2H), 2.66 (d, J = 19.5 Hz, 2H), 2.44 (s, 3H), 2.11 (s, 3H), 1.87 (s, 2H), 1.70 (d, J = 4.7 Hz, 2H), 1.47 (d, J = 4.7 Hz, 2H); ^{13}C NMR (126 MHz, DMSO) δ 168.78, 168.53, 159.44, 157.72, 154.60, 138.57, 130.09, 129.53, 129.47, 128.41, 118.57, 108.18, 41.23, 26.83, 24.78, 22.60, 22.20, 11.64, 10.58; HR-ESI-MS *m/z*: calcd for $C_{22}H_{22}N_3O_2S\{[M+H]^+\}$392.1433, found 392.1477.

*4.1.5.4. 1-((3,5-dimethylisoxazol-4-yl)methyl)-4-phenyl-1,5,6,7,8,9-hexahydro-2H-cyclohepta[4,5]thieno[2,3-d] pyrimidin-2-one **(3d)***. Rufous solid, yield 72%, m.p. 159.8–161.5 °C; ^{1}H NMR (500 MHz, $CDCl_3$) δ 7.38 (d, J = 6.9 Hz, 2H), 7.27 (dd, J = 15.9, 8.6 Hz, 3H), 5.03 (s, 2H), 2.59 (d, J = 4.1 Hz, 2H), 2.31 (s, 3H), 2.06 (s, 3H), 2.05–1.99 (m, 2H), 1.60 (s, 2H), 1.50 (s, 2H), 1.24 (s, 2H); ^{13}C NMR (126 MHz, $CDCl_3$) δ 168.82, 168.07, 159.13, 155.51, 154.85, 137.72, 135.28, 132.77, 130.12, 128.59, 127.92, 119.75, 107.40, 40.70, 31.72, 29.14, 28.82, 27.01, 26.38, 11.58, 10.53; HR-ESI-MS *m/z*: calcd for $C_{23}H_{24}N_3O_2S\{[M+H]^+\}$406.1589, found 406.1597.

*4.1.5.5. 1-(2-oxopropyl)-4-phenyl-5,6,7,8-tetrahydrobenzo[4,5]thieno[2,3-d]pyrimidin-2(1H)-one **(3e)***. Yellow solid, yield 77%, m.p. 234.4–236.6 °C; ^{1}H NMR (500 MHz, DMSO) δ 7.56–7.47 (m, 5H), 5.08 (d, J = 11.6 Hz, 2H), 2.69 (s, 2H), 2.32 (s, 3H), 1.90 (s, 2H), 1.72 (d, J = 4.3 Hz, 2H), 1.49 (d, J = 4.7 Hz, 2H); ^{13}C NMR (126 MHz, DMSO) δ 200.96, 169.05, 159.62, 154.25, 138.50, 130.13, 129.83, 129.24, 128.47, 128.34, 118.05, 57.93, 28.03, 26.91, 24.81, 22.59, 22.18; HR-ESI-MS *m/z*: calcd for $C_{19}H_{19}N_2O_2S\{[M+H]^+\}$339.1167, found 339.1189.

*4.1.5.6. 1-(3-oxobutan-2-yl)-4-phenyl-5,6,7,8-tetrahydrobenzo[4,5]thieno[2,3-d]pyrimidin-2(1H)-one **(3f)***. Yellow solid, yield 62%, m.p. 227.5–230.2 °C; ^{1}H NMR (500 MHz, DMSO) δ 7.50 (s, 5H), 4.88 (d, J = 6.4 Hz, 1H), 2.76 (d, J = 35.3 Hz, 2H), 2.07 (d, J = 37.4 Hz, 3H), 1.90 (s, 2H), 1.74 (s, 2H), 1.55 (t, J = 11.0 Hz, 3H), 1.49 (s, 2H); ^{13}C NMR (126 MHz, DMSO) δ 201.44, 169.24, 159.12, 153.59, 138.47, 130.19, 130.13, 129.36, 128.42, 118.78, 65.68, 26.94, 26.53, 24.84, 22.61, 22.20, 12.90; HR-ESI-MS *m/z*: calcd for $C_{20}H_{21}N_2O_2S\{[M+H]^+\}$353.1324, found 353.1371.

*4.1.5.7. N-methyl-2-(2-oxo-4-phenyl-5,6,7,8-tetrahydrobenzo[4,5]thieno[2,3-d]pyrimidin-1(2H)-yl)acetamide **(3g)***. Brown solid, yield 89%, m.p. 173.4–175.2 °C; ^{1}H NMR (500 MHz, DMSO) δ 8.01 (d, J = 3.6 Hz, 1H), 7.61–7.45 (m, 5H), 4.81 (s, 2H), 2.81 (s, 2H), 2.63 (d, J = 4.4 Hz, 3H), 2.05 (s, 2H), 1.79 (d, J = 4.1 Hz, 2H), 1.56 (d, J = 5.1 Hz, 2H); ^{13}C NMR (126 MHz, DMSO) δ 171.00, 168.21, 162.79, 160.21, 138.32, 134.83, 129.93, 129.36, 128.36, 127.11, 124.53, 66.03, 27.10, 25.81, 25.74, 22.63, 22.40; HR-ESI-MS *m/z*: calcd for $C_{19}H_{20}N_3O_2S\{[M+H]^+\}$354.1276, found 354.1284.

*4.1.5.8. 1-methyl-4-phenyl-5,6,7,8-tetrahydrobenzo[4,5]thieno[2,3-d]pyrimidin-2(1H)-one **(3h)***. Yellow solid, yield 92%, m.p. 278.4–280.1 °C; ^{1}H NMR (500 MHz, DMSO) δ 7.61 (t, J = 9.9 Hz, 3H), 7.53 (d, J = 6.6 Hz, 2H), 3.16 (s, 3H), 2.58 (s, 2H), 1.65 (s, 2H), 1.43 (d, J = 11.6 Hz, 4H); ^{13}C NMR (126 MHz, DMSO) δ 177.20, 154.06, 153.58, 132.01, 131.94, 130.80, 129.24, 128.66, 126.49, 117.50, 35.31, 25.53, 24.94, 22.09; HR-ESI-MS *m/z*: calcd for $C_{17}H_{17}N_2OS\{[M+H]^+\}$297.1062, found 297.1071.

*4.1.5.9. Methyl 1-((3,5-dimethylisoxazol-4-yl)methyl)-2-oxo-4-phenyl-1,2,5,6,7,8-hexahydrobenzo[4,5]thieno[2,3-d] pyrimidine-7-carboxylate **(3i)***. White solid, yield 62%, m.p. 94.1–96.1 °C; ^{1}H NMR (500 MHz, DMSO) δ 7.58–7.45 (m, 5H), 5.19 (dd, J = 68.6, 15.7 Hz, 2H), 3.61 (s, 3H), 2.98 (d, J = 12.6 Hz, 1H), 2.89–2.80 (m, 2H), 2.46 (s, 3H), 2.12 (s, 3H), 2.08 (s, 1H), 1.83 (d, J = 16.2 Hz, 2H), 1.53 (d, J = 8.4 Hz, 1H); ^{13}C NMR (126 MHz, DMSO) δ 174.51, 168.78, 168.63, 159.44, 157.95, 154.57, 138.41, 130.19, 128.99, 128.46, 128.43, 127.78, 118.15, 108.12, 52.20, 41.15, 38.75, 26.95, 25.67, 24.94, 11.65, 10.57; HR-ESI-MS *m/z*: calcd for $C_{24}H_{24}N_3O_4S\{[M+H]^+\}$450.1488, found 450.1500.

*4.1.5.10. 1-((3,5-dimethylisoxazol-4-yl)methyl)-7,7-dimethyl-4-phenyl-5,6,7,8-tetrahydrobenzo[4,5]thieno[2,3-d] pyrimidin-2(1H)-one **(3j)***. White solid, yield 79%, m.p. 180.0–182.6 °C; ^{1}H NMR (500 MHz, DMSO) δ 7.56–7.48 (m, 5H), 5.19 (s, 2H), 2.47 (s, 2H), 2.45 (s, 3H), 2.12 (s, 3H), 1.88 (s, 2H), 1.25 (s, 2H), 0.92 (s, 6H); ^{13}C NMR (126 MHz, DMSO) δ 168.83, 168.56, 159.45, 157.77, 154.60, 138.58, 130.06, 128.88, 128.44, 128.38, 128.02, 118.36, 108.20, 41.12, 38.17, 34.88, 30.23, 27.84, 24.28, 11.65, 10.59; HR-ESI-MS *m/z*: calcd for $C_{24}H_{26}N_3O_2S\{[M+H]^+\}$ 420.1746, found 420.1752.

*4.1.5.11. 4-(4-chlorophenyl)-1-((3,5-dimethylisoxazol-4-yl)methyl)-7-phenyl-5,6,7,8-tetrahydrobenzo[4,5]thieno[2,3-d] pyrimidin-2(1H)-one **(3k)***. Yellow solid, yield 90%, m.p. 123.1–125.6 °C; ^{1}H NMR

(500 MHz, DMSO) δ 7.60–7.52 (m, 4H), 7.28 (dt, J = 14.7, 7.4 Hz, 4H), 7.20 (t, J = 7.0 Hz, 1H), 5.19 (dd, J = 78.7, 15.8 Hz, 2H), 3.03–2.90 (m, 2H), 2.83–2.73 (m, 1H), 2.44 (d, J = 10.6 Hz, 3H), 2.34–2.25 (m, 1H), 2.14 (d, J = 12.9 Hz, 3H), 1.92–1.76 (m, 2H), 1.63 (qd, J = 12.2, 4.9 Hz, 1H); ^{13}C NMR (126 MHz, DMSO) 168.59, 167.57, 159.45, 158.28, 154.51, 145.60, 137.25, 135.01, 130.53, 129.40, 129.05, 128.88, 128.59, 127.23, 126.84, 118.25, 108.12, 41.32, 40.04, 32.46, 29.62, 27.36, 11.66, 10.60; HR-ESI-MS *m/z*: calcd for $C_{28}H_{25}ClN_3O_2S$ {[M + H]$^+$}502.1356, found 502.1357.

4.1.5.12. 4-(4-chlorophenyl)-1-((2-chlorothiazol-5-yl)methyl)-7-phenyl-5,6,7,8-tetrahydrobenzo[4,5]thieno[2,3-d] pyrimidin-2(1H)-one ***(3l)***. Yellow solid, yield 79%, m.p. 203.9–205.0 °C; ^{1}H NMR (500 MHz, DMSO) δ 7.93 (s, 1H), 7.56 (dd, J = 21.3, 8.4 Hz, 4H), 7.34–7.25 (m, 4H), 7.22 (t, J = 6.9 Hz, 1H), 5.43 (s, 2H), 3.07–2.95 (m, 2H), 2.89–2.82 (m, 1H), 2.28 (d, J = 11.6 Hz, 1H), 1.89–1.79 (m, 2H), 1.65 (dt, J = 11.6, 7.3 Hz, 1H); ^{13}C NMR (126 MHz, DMSO) δ 168.06, 158.25, 154.13, 152.51, 145.61, 143.05, 137.20, 135.05, 133.85, 130.47, 129.61, 128.92, 128.63, 127.30, 126.88, 118.45, 45.70, 40.60, 32.49, 29.63, 27.34; HR-ESI-MS *m/z*: calcd for $C_{26}H_{20}Cl_2N_3OS_2$ {[M + H]$^+$}524.0425, found 524.0420.

4.1.5.13. 1-((3,5-dimethylisoxazol-4-yl)methyl)-7-isopropyl-4-(4-methoxyphenyl)-5,6,7,8- Tetrahydropyrido [4′,3′:4,5]thieno[2,3-d] pyrimidin-2(1H)-one ***(3m)***. Brown solid, yield 86%, m.p. 69.1–71.6 °C; ^{1}H NMR (500 MHz, DMSO) δ 7.49 (t, J = 8.4 Hz, 2H), 7.05 (d, J = 8.4 Hz, 2H), 5.18 (s, 2H), 3.84 (s, 3H), 3.63 (s, 2H), 2.80 (dt, J = 13.0, 6.5 Hz, 1H), 2.44 (s, 3H), 2.15 (dd, J = 15.7, 6.8 Hz, 2H), 2.10 (s, 3H), 1.59 (d, J = 6.2 Hz, 2H), 0.98 (t, J = 10.3 Hz, 6H); ^{13}C NMR (126 MHz, DMSO) δ 168.47, 161.11, 159.42, 157.91, 154.71, 130.62, 130.52, 128.52, 127.94, 118.07, 114.91, 113.82, 108.18, 55.75, 53.78, 47.10, 45.79, 41.12, 18.73, 14.41, 11.61, 10.54; HR-ESI-MS *m/z*: calcd for $C_{25}H_{29}N_4O_3S$ {[M + H]$^+$}465.1960, found 465.1963.

4.1.5.14. 7-(tert-butyl)-1-((3,5-dimethylisoxazol-4-yl)methyl)-4-phenyl-5,6,7,8-tetrahydrobenzo[4,5]thieno[2,3-d] pyrimidin-2(1H)-one ***(3n)***. White solid, yield 74%, m.p. 245.8–247.6 °C; ^{1}H NMR (500 MHz, DMSO) δ 7.51 (dd, J = 16.4, 8.4 Hz, 5H), 5.19 (dd, J = 86.0, 15.7 Hz, 2H), 2.76 (d, J = 14.6 Hz, 1H), 2.45 (s, 3H), 2.41 (d, J = 15.4 Hz, 1H), 2.12 (s, 3H), 2.07 (d, J = 13.2 Hz, 1H), 1.74 (dd, J = 25.9, 13.8 Hz, 2H), 1.43 (t, J = 9.5 Hz, 1H), 0.99 (dd, J = 16.9, 7.7 Hz, 1H), 0.85 (s, 9H);^{13}C NMR (126 MHz, DMSO) δ 168.69, 168.57, 159.43, 157.91, 154.64, 138.46, 130.25, 130.12, 129.45, 128.47, 128.43, 118.26, 108.17, 44.61, 41.14, 32.62, 27.80, 27.41, 26.57, 23.96, 11.64, 10.57; HR-ESI-MS *m/z*: calcd for $C_{26}H_{30}N_3O_2S$ {[M + H]$^+$}448.2059, found 448.2067.

4.1.5.15. 7-(tert-butyl)-4-(4-chlorophenyl)-1-((3,5-dimethylisoxazol-4-yl) methyl)-5,6,7,8-tetrahydrobenzo[4,5]thieno [2,3-d]pyrimidin-2(1H)-one ***(3o)***. Yellow solid, yield 89%, m.p. 154.2–156.1 °C; ^{1}H NMR (500 MHz, DMSO) δ 7.56 (dd, J = 21.8, 8.5 Hz, 4H), 5.29–5.08 (m, 2H), 2.77 (dd, J = 16.7, 4.7 Hz, 1H), 2.45 (s, 3H), 2.44–2.37 (m, 1H), 2.11 (s, 3H), 2.11–2.05 (m, 1H), 1.79 (t, J = 11.1 Hz, 2H), 1.44 (td, J = 11.7, 4.4 Hz, 1H), 1.00 (dt, J = 12.3, 7.5 Hz, 1H), 0.86 (s, 9H); ^{13}C NMR (126 MHz, DMSO) δ 168.64, 167.42, 159.45, 158.17, 154.54, 137.22, 134.97, 130.56, 130.45, 129.25, 128.56, 118.20, 108.12, 44.60, 41.17, 32.63, 27.91, 27.41, 26.59, 23.97, 11.65, 10.59; HR-ESI-MS *m/z*: calcd for $C_{26}H_{29}ClN_3O_2S$ {[M + H]$^+$}482.1669, found 482.1673.

4.1.5.16. 7-(tert-butyl)-1-((3,5-dimethylisoxazol-4-yl)methyl)-4-(4-methoxyphenyl)-5,6,7,8-tetrahydrobenzo[4,5]thieno [2,3-d]pyrimidin-2(1H)-one ***(3p)***. Yellow solid, yield 67%, m.p. 120.1–122.6 °C; ^{1}H NMR (400 MHz, DMSO) δ 7.47 (d, J = 8.6 Hz, 2H), 7.05 (d, J = 8.7 Hz, 2H), 5.18 (dd, J = 93.1, 15.8 Hz, 2H), 3.84 (s, 3H), 2.77 (dd, J = 16.6, 4.3 Hz, 1H), 2.46 (d, J = 7.8 Hz, 1H), 2.43 (d, J = 16.5 Hz, 3H), 2.26–2.17 (m, 1H), 2.10 (s, 3H), 1.83 (dd, J = 43.7, 14.0 Hz, 2H), 1.47 (dd, J = 11.1, 6.7 Hz, 1H), 1.05–0.96 (m, 1H), 0.86 (s, 9H); ^{13}C NMR (126 MHz, DMSO) δ 168.51, 168.28, 161.02, 159.39, 157.78, 154.64, 130.68, 130.56, 130.06, 129.64, 118.24, 113.73, 108.23, 55.72, 44.64, 40.96, 32.61, 28.27, 27.37, 26.63, 24.06, 11.61, 10.55. HR-ESI-MS *m/z*: calcd for $C_{27}H_{32}N_3O_3S$ {[M + H]$^+$}478.2146, found 478.2170.

4.1.5.17. methyl 4-(7-(tert-butyl)-1-((3,5-dimethylisoxazol-4-yl)methyl)-2-oxo-1,2,5,6,7,8-hexahydrobenzo [4,5]thieno [2,3-d]pyrimidin-4-yl) benzoate ***(3q)***. Yellow solid, yield 64%, m.p. 208.1–210.6 °C; ^{1}H NMR (500 MHz, DMSO) δ 8.08 (d, J = 8.1 Hz, 2H), 7.64 (d, J = 8.0 Hz, 2H), 5.29–5.10 (m, 2H), 3.90 (s, 3H), 2.76 (dd, J = 16.6, 4.3 Hz, 1H), 2.45 (s, 3H), 2.40 (d, J = 13.9 Hz, 1H), 2.10 (d, J = 14.6 Hz, 3H), 2.05 (t, J = 13.1 Hz, 1H), 1.72 (d, J = 11.2 Hz, 2H), 1.42 (td, J = 11.7, 4.5 Hz, 1H), 0.97 (qd, J = 12.6, 4.3 Hz, 1H), 0.84 (s, 9H); ^{13}C NMR (126 MHz, DMSO) δ 168.64, 167.58, 166.28, 159.44, 158.29, 154.50, 142.74, 130.93, 130.57, 129.31, 129.15, 128.99, 118.14, 108.09, 52.82, 44.59, 41.26, 32.60, 27.71, 27.39, 26.56, 23.91, 11.65, 10.58; HR-ESI-MS *m/z*: calcd for $C_{28}H_{32}N_3O_4S$ {[M + H]$^+$}506.2114, found 506.2111.

4.1.5.18. 7-(tert-butyl)-1-((3,5-dimethylisoxazol-4-yl)methyl)-4-(4-fluorophenyl)-5,6,7,8-tetrahydrobenzo[4,5]thieno [2,3-d]pyrimidin-2(1H)-one ***(3r)***. Yellow solid, yield 92%, m.p. 241.4–243.4 °C; ^{1}H NMR (500 MHz, DMSO) δ 7.56 (dd, J = 8.0, 5.7 Hz, 2H), 7.33 (t, J = 8.7 Hz, 2H), 5.18 (dd, J = 98.8, 15.7 Hz, 2H), 2.76 (dd, J = 16.6, 4.1 Hz, 1H), 2.45 (s, 3H), 2.41 (d, J = 14.3 Hz, 1H), 2.13 (d, J = 14.7 Hz, 1H), 2.11 (s, 3H), 1.85–1.70 (m, 2H), 1.43 (td, J = 11.7, 4.3 Hz, 1H), 1.00 (tt, J = 12.1, 5.9 Hz, 1H), 0.85 (s, 9H); ^{13}C NMR (126 MHz, DMSO) δ 168.59, 167.63, 164.33, 162.37, 159.42, 158.04, 154.56, 134.86, 131.10, 131.04, 130.33, 129.37, 118.29, 115.54, 115.36, 108.15, 44.62, 41.12, 32.61, 27.94, 27.39, 26.59, 24.00, 11.64, 10.57; HR-ESI-MS *m/z*: calcd for $C_{26}H_{29}FN_3O_2S$ {[M + H]$^+$} 466.1965, found 466.1960.

4.1.5.19. 7-(tert-butyl)-4-(3-chlorophenyl)-1-((3,5-dimethylisoxazol-4-yl) methyl)-5,6,7,8-tetrahydrobenzo[4,5]thieno [2,3-d]pyrimidin-2(1H)-one ***(3s)***. Yellow solid, yield 79%, m.p. 198.8–201.0 °C; ^{1}H NMR (500 MHz, DMSO) δ 7.60 (t, J = 5.9 Hz, 1H), 7.57 (d, J = 13.5 Hz, 1H), 7.53 (t, J = 7.7 Hz, 1H), 7.46 (d, J = 7.5 Hz, 1H), 5.30–5.07 (m, 2H), 2.77 (dd, J = 16.5, 3.9 Hz, 1H), 2.45 (s, 3H), 2.41 (d, J = 14.3 Hz, 1H), 2.10 (d, J = 12.7 Hz, 3H), 2.09–2.00 (m, 1H), 1.86–1.71 (m, 2H), 1.47–1.40 (m, 1H), 1.01 (dt, J = 13.2, 8.5 Hz, 1H), 0.85 (s, 9H); ^{13}C NMR (126 MHz, DMSO) δ 168.64, 166.96, 159.44, 158.23, 154.50, 140.36, 133.21, 130.52, 130.43, 129.98, 129.16, 128.25, 127.28, 118.18, 108.10, 44.57, 41.21, 32.62, 27.74, 27.40, 26.56, 23.96, 11.65, 10.58; HR-ESI-MS *m/z*: calcd for $C_{26}H_{29}ClN_3O_2S$ {[M + H]$^+$} 482.1669, found 482.1671.

4.1.5.20. 7-(tert-butyl)-4-(2-chlorophenyl)-1-((3,5-dimethylisoxazol-4-yl) methyl)-5,6,7,8-tetrahydrobenzo[4,5]thieno [2,3-d]pyrimidin-2(1H)-one ***(3t)***. Yellow solid, yield 75%, m.p. 108.1–110.6 °C; ^{1}H NMR (500 MHz, DMSO) δ 7.70–7.40 (m, 4H), 5.22 (dt, J = 34.5, 15.7 Hz, 2H), 2.74 (t, J = 14.0 Hz, 1H), 2.44 (d, J = 2.1 Hz, 3H), 2.38 (d, J = 17.1 Hz, 1H), 2.06 (d, J = 35.4 Hz, 3H), 2.03–1.89 (m, 1H), 1.77–1.66 (m, 2H), 1.39–1.30 (m, 1H), 1.03 (ddd, J = 20.0, 14.5, 6.9 Hz, 1H), 0.80 (d, J = 32.4 Hz, 9H); ^{13}C NMR (126 MHz, DMSO) δ 168.39, 165.92, 159.17, 157.53, 154.71, 137.31, 131.57, 131.04, 130.69, 129.76, 129.66, 128.95, 127.83, 118.79, 108.03, 44.56, 41.33, 32.67, 27.42, 26.36, 25.18, 23.58, 11.61, 10.40; HR-ESI-MS *m/z*: calcd for $C_{26}H_{29}ClN_3O_2S$ {[M + H]$^+$}482.1669, found 482.1669.

4.1.5.21. 7-(tert-butyl)-4-(3,4-dichlorophenyl)-1-((3,5-dimethylisoxazol-4-yl)methyl)-5,6,7,8-tetrahydrobenzo[4,5] thieno[2,3-d]pyrimidin-2(1H)-one ***(3u)***. Yellow solid, yield 93%, m.p. 202.1–204.4 °C; ^{1}H NMR (500 MHz, DMSO) δ 7.81 (t, J = 4.9 Hz, 1H), 7.77 (d, J = 8.2 Hz, 1H), 7.51 (dd, J = 8.2, 1.4 Hz, 1H), 5.19 (dd, J = 89.6, 15.7 Hz, 2H),

2.77 (dd, J = 16.6, 4.2 Hz, 1H), 2.45 (s, 3H), 2.41 (d, J = 14.2 Hz, 1H), 2.11 (s, 3H), 2.06 (s, 1H), 1.88–1.76 (m, 2H), 1.43 (td, J = 11.6, 4.3 Hz, 1H), 1.05–0.96 (m, 1H), 0.86 (d, J = 9.1 Hz, 9H); ^{13}C NMR (126 MHz, DMSO) δ 168.69, 165.91, 159.45, 158.41, 154.41, 138.82, 132.93, 131.38, 130.80, 130.64, 130.59, 129.06, 128.99, 118.16, 108.06, 44.56, 41.21, 32.62, 27.85, 27.39, 26.58, 23.97, 11.66, 10.60; HR-ESI-MS *m/z*: calcd for $C_{26}H_{28}Cl_2N_3O_2S\{[M+H]^+\}$516.1279, found 516.1274.

4.1.5.22. 7-(tert-butyl)-4-phenyl-1-(pyrimidin-2-ylmethyl)-5,6,7,8-tetrahydrobenzo[4,5]thieno[2,3-d]pyrimidin-2(1H)-one ***(3v)***. Yellow solid, yield 78%, m.p. 185.5–186.3 °C; ^{1}H NMR (500 MHz, DMSO) δ 8.77 (d, J = 4.8 Hz, 2H), 7.55–7.36 (m, 6H), 5.69–5.56 (m, 2H), 2.81 (dd, J = 16.9, 3.7 Hz, 1H), 2.52 (d, J = 11.8 Hz, 1H), 2.24 (t, J = 13.0 Hz, 1H), 1.87 (d, J = 15.0 Hz, 1H), 1.76 (d, J = 11.4 Hz, 1H), 1.55–1.44 (m, 1H), 1.06–0.97 (m, 1H), 0.85 (s, 9H); ^{13}C NMR (126 MHz, DMSO) δ 171.28, 165.80, 162.55, 160.56, 157.80, 138.19, 135.32, 129.89, 129.34, 128.32, 127.00, 124.03, 120.61, 68.80, 44.54, 32.58, 28.10, 27.50, 27.38, 24.10; HR-ESI-MS *m/z*: calcd for $C_{25}H_{27}N_4OS\{[M+H]^+\}$431.1906, found 431.1898.

4.1.5.23. 7-(tert-butyl)-1-((2-chlorothiazol-5-yl)methyl)-4-phenyl-5,6,7,8-tetrahydrobenzo[4,5]thieno[2,3-d]pyrimidin-2(1H)-one ***(3w)***. White solid, yield 90%, m.p. 225.2–226.7 °C; ^{1}H NMR (500 MHz, DMSO) δ 7.92 (s, 1H), 7.56–7.45 (m, 5H), 5.45–5.38 (m, 2H), 2.78 (dd, J = 16.5, 4.4 Hz, 1H), 2.45 (d, J = 13.5 Hz, 1H), 2.07 (t, J = 14.2 Hz, 1H), 1.73 (t, J = 14.5 Hz, 2H), 1.45 (td, J = 11.5, 4.2 Hz, 1H), 0.97 (tt, J = 11.4, 5.8 Hz, 1H), 0.85 (s, 9H); ^{13}C NMR (126 MHz, DMSO) δ 169.16, 157.94, 154.22, 152.50, 143.04, 138.34, 133.91, 130.46, 130.20, 130.05, 128.46, 128.43, 118.44, 45.61, 44.60, 32.63, 27.83, 27.40, 26.62, 23.91; HR-ESI-MS *m/z*: calcd for $C_{24}H_{25}ClN_3OS_2\{[M+H]^+\}$470.1128, found 470.1133.

4.1.5.24. 7-(tert-butyl)-1-((2-chlorothiazol-5-yl)methyl)-4-(4-methoxyphenyl)-5,6,7,8-tetrahydrobenzo[4,5]thieno[2,3-d]pyrimidin-2(1H)-one ***(3x)***. White solid, yield 91%, m.p. 239.9–241.7 °C; ^{1}H NMR (500 MHz, DMSO) δ 7.91 (s, 1H), 7.45 (d, J = 8.6 Hz, 2H), 7.04 (d, J = 8.7 Hz, 2H), 5.44–5.34 (m, 2H), 3.83 (s, 3H), 2.77 (dd, J = 16.5, 4.4 Hz, 1H), 2.49–2.40 (m, 1H), 2.20 (t, J = 13.9 Hz, 1H), 1.80 (dd, J = 55.4, 13.8 Hz, 2H), 1.46 (td, J = 11.6, 4.6 Hz, 1H), 0.97 (tt, J = 12.2, 6.2 Hz, 1H), 0.85 (s, 9H); ^{13}C NMR (126 MHz, DMSO) δ 168.76, 161.08, 157.82, 154.25, 152.49, 143.01, 133.98, 130.57, 130.53, 130.29, 130.26, 118.42, 113.80, 55.74, 45.52, 44.64, 32.63, 28.30, 27.38, 26.68, 24.02; HR-ESI-MS *m/z*: calcd for $C_{25}H_{27}ClN_3O_2S_2\{[M+H]^+\}$500.1233, found 500.1238.

4.1.5.25. 7-(tert-butyl)-4-(4-chlorophenyl)-1-((2-chlorothiazol-5-yl)methyl)-5,6,7,8-tetrahydrobenzo[4,5]thieno[2,3-d]pyrimidin-2(1H)-one ***(3y)***. Yellow solid, yield 65%, m.p. 270.3–272.1 °C; ^{1}H NMR (500 MHz, DMSO) δ 7.91 (s, 1H), 7.61–7.49 (m, 4H), 5.41 (s, 2H), 2.79 (dd, J = 16.4, 4.1 Hz, 1H), 2.46 (d, J = 14.0 Hz, 1H), 2.11 (t, J = 13.7 Hz, 1H), 1.78 (d, J = 15.2 Hz, 2H), 1.48–1.41 (m, 1H), 1.03–0.95 (m, 1H), 0.87 (d, J = 17.5 Hz, 9H); ^{13}C NMR (126 MHz, DMSO) δ 167.88, 158.20, 154.13, 152.51, 143.06, 137.09, 135.06, 133.83, 130.63, 130.51, 129.86, 128.60, 118.38, 45.63, 44.60, 32.62, 27.95, 27.39, 26.64, 23.92; HR-ESI-MS *m/z*: calcd for $C_{24}H_{24}Cl_2N_3OS_2\{[M+H]^+\}$ 504.0738, found 504.0740.

4.1.5.26. 4-(((7-(tert-butyl)-4-(3,4-dichlorophenyl)-5,6,7,8-tetrahydrobenzo[4,5]thieno[2,3-d]pyrimidin-2-yl)oxy)methyl)-3,5-dimethylisoxazole ***(3z)***. White solid, yield 88%, m.p. 80.7–82.6 °C; ^{1}H NMR (500 MHz, DMSO) δ 7.84 (s, 1H), 7.78 (d, J = 8.0 Hz, 1H), 7.52 (d, J = 8.1 Hz, 1H), 5.33–5.22 (m, 2H), 2.85 (d, J = 15.4 Hz, 1H), 2.60–2.51 (m, 1H), 2.39 (d, J = 15.3 Hz, 3H), 2.24 (s, 3H), 2.19 (s, 1H), 1.95 (d, J = 15.3 Hz, 1H), 1.84 (d, J = 11.3 Hz, 1H), 1.51 (d, J = 9.9 Hz, 1H), 1.07 (d, J = 9.8 Hz, 1H), 0.87 (s, 9H); ^{13}C NMR (126 MHz, DMSO) δ 171.48, 168.62, 160.23, 160.11, 160.05, 138.62, 136.01, 132.83, 131.33, 130.66, 129.85, 126.76, 124.10, 110.59, 100.04, 58.59, 44.51, 32.62, 28.02, 27.53, 27.39, 24.11, 11.31, 10.15; HR-ESI-MS *m/z*: calcd for $C_{26}H_{28}Cl_2N_3O_2S\{[M+H]^+\}$ 516.1279, found 516.1277.

4.2. Docking study

All ligands were drawn in ChemDraw 2014, and saved as sdf style. Ligand molecules were prepared using the MOE2018 to get low-energy 3D conformations. Protein (PDB code: 2YEM, 2YEL) was retrieved from RSCB database and prepared using the protein preparation wizard from MOE2018. Molecular docking was performed using a flexible ligand and fixed receptor models. Ligand conformations are generated with the bond rotation method. These are then placed in the site with the Triangle Matcher method, and ranked with the London dG scoring function. The Retain option specifies the number of poses (2 0 0) to pass to the Refinement, for energy minimization in the pocket, before re-scoring with the GBVI/WSA dG scoring function. At last, only the best-scoring ligand protein complexes were kept for analyses

4.3. Biological evaluation

4.3.1. Binding affinity of target compounds to BRD4-BD1 and BRD4-BD2 by AlphaScreen assay.

The bead-based Amplifed Luminescent Proximity Homogeneous Assay (ALPHA) was used to measure the binding of a tetra-acetylated histone H4 tail peptide to BRD4 BD1 and BD2. BRD4(1) (No. AL609C, Perkin Elmer), BRD4(2) (No. AL610C, Perkin Elmer), (+)-JQ1(No. BD229144, Bidepharm), RVX-208(No. BD229143, Bidepharm). Prepare 1X Alpha Assay Buffer (50 mM HEPES, 01% BSA); serial dilution of sample (Preparation of 10X of compound dilutions in 1X Assay Buffer, final concentration of DMSO in these compound dilutions will be 1%, start from 100 μM and 1:5 dilution); 5X BRD4(BD1 or BD2); 5X H4 K5,8,12,16Ac; 4X Histidine Conjugated Acceptor Beads with 1X Assay Buffer and 4X Streptavidin (SA) Donor Beads with 1X Assay Buffer. Transfer 2 μl compounds to 384 assay plates. Then mix 4 μl BRD4(BD1 or BD2), 4 μl H4 K5,8,12,16Ac and 5 μl Histidine Conjugated Acceptor Beads. Incubate at room temperature for 60 min. At last, add 5ul SA-Donor Beads and incubate 30 min at RT in the dark. Read endpoint with Bio Tek Cytation™ 5 Cell Imaging Multi-Mode Reader with Alpha mode. The IC_{50} was calculated by GraphPad Prism 5 statistical software.

4.3.2. Cell culture

MCF-7 cells, A549 cells and HT-29 cells were cultured in RPMI 1640 supplemented with 10% FBS and penicillin/streptomycin mixture. HepG2 cells, A375 cells, NRK-49F cells and LX-2 cells were cultured in D-MEM (High Glucose) supplemented with 10% FBS and penicillin/streptomycin mixture. HLF-1 cells were cultured in D-MEM/F-12(1:1) supplemented with 10% FBS and penicillin/streptomycin mixture. All cells were incubated at 37 °C in a humidified incubator (5% CO_2 in air).

4.3.3. Cell proliferative inhibition assay

Briefly, cells were seeded into 96-well plates at a density appropriate for exponential growth at the start of the assay, and treated with a range of concentrations of compounds for 48 h. Fresh MTT (10 μl) was added to each well and incubated at 37 °C for 4 h. The formazan crystals in each well were dissolved in 150 μl DMSO. The spectrophotometric absorbance of each well was measured by a multi-detection microplate reader at a wavelength of 490 nm. The IC_{50} was calculated by GraphPad Prism 5 statistical software.

4.3.4. Western blot analysis

A375 or HLF-1 cells (2.5×10^5 cells/well) incubated in 6-well plates were treated with compounds for 24 h. The treated cells were collected, lysed on ice, and then centrifuged at 4 °C, 12,000g, 15 min,

leaving the supernatant. The protein concentration was measured with BCA Protein Assay kit (No. BL521A, Biosharp). 20–40 μg protein was electrophoresed on SDS-PAGE and transferred to PVDF membranes. The membrane was blocked with 5% skim milk, and incubated with primary antibodies c-myc (No. 13987, Cell Signaling), collagen I (No. 34710, Abcam) and β-Actin (No. 4970, Cell Signaling) overnight. Then it was incubated with the appropriate secondary antibodies (No. A21020, Abbkine) for 1 h. At last, the bands were detected by western fluorescent detection reagent (No. WBKLS0100, Millipore) and imaged within the ChemiDoc XRS^{+c} imaging system.

4.3.5. RNA isolation and quantitative RT-PCR

A375 or HLF-1 cells (2.5×10^5 cells/well) incubated in 6-well plates were treated with compounds for 24 h. Total RNA were extracted using Total RNA Extraction Reagent (No. RN01005S, Monad) according to the manufacturer's instructions. cDNA was synthesized from total RNA using MonScript™ RTIII all-in-one Mix (No. RN05004S, Monad). Expression levels of specific genes were quantified by real-time PCR (No. 788BR07164, CFX Connect™ Optics Module) using MonAmp™ ChemoHS qPCR Mix (No. RN04001M, Monad). The primer sequences are shown below.

Gene	Primer sequence (5′–3′)
c-Myc Forward	*GGCTCCTGGCAAAAGGTCA*
C-Myc Reverse	*CTGCGTAGTTGTGCTGATGT*
Collagen I Forward	*CAGCCGCTTCACCTACAGC*
Collagen I Reverse	*TTTTGTATTCAATCACTGTCTTGCC*

4.3.6. Cell apoptosis

A375 cells (1×105 cells/well) incubated in 24-well plates were treated with compounds for 24 h. After 24 h, cell apoptosis was determined by using the Annexin V-FITC Apoptosis Detection Kit (No. A211-01, Vazyme). Briefly, the cells were washed twice with ice-cold PBS, and then 6 μL of Annexin V-FITC and 3 μL of PI were applied to stain cells. After incubated for 15 min at room temperature in dark, the stained cells were analyzed using fluorescence microscope (Bio Tek Cytation™ 5 Cell Imaging Multi-Mode Reader, USA).

Acknowledgments

This work was supported by the National Natural Science Foundation of China (No. 81573287 & 81773640), Hunan Province Strategic Emerging Industry Science and Technology Key Project (No. 2016GK4028) and Postgraduates innovation subject of Central South University (No. 2018zzts875). Key research and development project of Hainan Province (project number: ZDYF2017092), Haikou, China. Hainan Province Key Research and Development Project (ZDYF2016128) Haikou, China. We also would like to thank the Nuclear Magnetic Resonance Laboratory of Advanced Research Center in Central South University for the technological assistance in chemical characterization.

Appendix A. Supplementary data

Supplementary data to this article can be found online at https://doi.org/10.1016/j.bmc.2019.03.037.

References

1. Jiang YW, Veschambre P, Erdjument-Bromage H, et al. Mammalian mediator of transcriptional regulation and its possible role as an endpoint of signal transduction pathways. *Proc Natl Acad Sci USA.* 1998;95:8538–8543.
2. Belkina AC, Denis GV. BET domain co-regulators in obesity, inflammation and cancer. *Nat Rev Cancer.* 2012;12:465–477.
3. Padmanabhan B, Mathur S, Manjula R, et al. Bromodomain and extra-terminal (BET) family proteins: new therapeutic targets in major diseases. *J Biosci.* 2016;41:295–311.
4. Ding N, Hah N, Yu RT, et al. BRD4 is a novel therapeutic target for liver fibrosis. *Proc Natl Acad Sci USA.* 2015;112:15713–15718.
5. Fukazawa H, Masumi A. The conserved 12-amino acid stretch in the inter-bromodomain region of BET family proteins functions as a nuclear localization signal. *Biol Pharm Bull.* 2012;35:2064–2068.
6. Jonkers I, Lis JT. Getting up to speed with transcription elongation by RNA polymerase II. *Nat Rev Mol Cell Biol.* 2015;16:167–177.
7. You JS, Han JH. Targeting components of epigenome by small molecules. *Arch Pharmacal Res.* 2014;37:1367–1374.
8. Wu X, Liu D, Tao D, et al. BRD4 regulates EZH2 transcription through upregulation of C-MYC and represents a novel therapeutic target in bladder cancer. *Mol Cancer Ther.* 2016;15:1029–1042.
9. Mertz JA, Conery AR, Bryant BM, et al. Targeting MYC dependence in cancer by inhibiting BET bromodomains. *Proc Natl Acad Sci USA.* 2011;108:16669–16674.
10. Delmore J, Issa G, Lemieux M, et al. BET Bromodomain Inhibition as a Therapeutic Strategy to Target c-Myc. *Cell.* 2011;146.
11. Dang Chi V. MYC, microRNAs and glutamine addiction in cancers. *Cell Cycle.* 2009;8:3243–3245.
12. Liu L, You Z, Yu H, et al. Mechanotransduction-modulated fibrotic microniches reveal the contribution of angiogenesis in liver fibrosis. *Nat Mater.* 2017;16:1252–1261.
13. Dhalluin C, Carlson JE, Zeng L, et al. Structure and ligand of a histone acetyltransferase bromodomain. *Nature.* 1999;399:491–496.
14. Owen DJ, Ornaghi P, Yang Ji-Chun, et al. The structural basis for the recognition of acetylated histone H4 by the bromodomain of histone acetyltransferase Gcn5p. *EMBO J.* 2000;19:6141–6149.
15. Morinière Jeanne, Rousseaux S, Steuerwald U, et al. Cooperative binding of two acetylation marks on a histone tail by a single bromodomain. *Nature.* 2009;461:664–668.
16. Filippakopoulos P, Picaud S, Mangos M, et al. Histone recognition and large-scale structural analysis of the human bromodomain family. *Cell.* 2012;149.
17. Gacias M, Gerona-Navarro G, Plotnikov AN, et al. Selective chemical modulation of gene transcription favors oligodendrocyte lineage progression. *Chem Biol.* 2014;21:841–854.
18. Lei-Lei F, Mao T, Xiang L, et al. Inhibition of BET bromodomains as a therapeutic strategy for cancer drug discovery. *Oncotarget.* 2015;6:5501–5516.
19. Vollmuth F, Blankenfeldt W, Geyer M. Structures of the dual bromodomains of the P-TEFb-activating protein Brd4 at atomic resolution. *J Biol Chem.* 2009;284:36547–36556.
20. Filippakopoulos P, Picaud S, Mangos M, et al. Histone recognition and large-scale structural analysis of the human bromodomain family. *Cell.* 2012;149:214–231.
21. Shi J, Wang Y, Zeng L, et al. Disrupting the interaction of BRD4 with diacetylated Twist suppresses tumorigenesis in basal-like breast cancer. *Cancer Cell.* 2014;25:210–225.
22. Albrecht BK, Gehling VS, Hewitt MC, et al. Identification of a benzoisoxazoloazepine inhibitor (CPI-0610) of the bromodomain and extra-terminal (BET) family as a candidate for human clinical trials. *J Med Chem.* 2016;59:1330–1339.
23. Picaud S, Wells C, Felletar I, et al. RVX-208, an inhibitor of BET transcriptional regulators with selectivity for the second bromodomain. *Proc Natl Acad Sci USA.* 2013;110:19754–19759.
24. Mar G, Guillermo GN, et al. Selective chemical modulation of gene transcription favors oligodendrocyte lineage progression. *Chem Biol.* 2014;21:841–854.
25. Filippakopoulos P, Qi J, Picaud S, et al. Selective inhibition of BET bromodomains. *Nature.* 2010;468:1067–1073.
26. Baud MG, Lin-Shiao E, Zengerle M, et al. New synthetic routes to triazolo-benzodiazepine analogues: expanding the scope of the bump-and-hole approach for selective bromo and extra-terminal (BET) bromodomain inhibition. *J Med Chem.* 2016;59:1492–1500.
27. Galdeano C, Ciulli A. Selectivity on-target of bromodomain chemical probes by structure-guided medicinal chemistry and chemical biology. *Future Med Chem.* 2016 fmc-2016-0059.
28. Sahni JM, Keri RA. Targeting bromodomain and extraterminal proteins in breast cancer. *Pharmacol Res.* 2017 S1043661817314032.
29. Bihani T, Ezell SA, Ladd B, et al. Resistance to everolimus driven by epigenetic regulation of MYC in ER+ breast cancers. *Oncotarget.* 2015;6:2407–2420.
30. Feng Q, Zhang Z, Shea MJ, et al. An epigenomic approach to therapy for tamoxifen-resistant breast cancer. *Cell Res.* 2014;24:809–819.